European Journal of Nuclear Medicine and Molecular Imaging (2021) 48:3129–3140
https://doi.org/10.1007/s00259-021-05249-8

ORIGINAL ARTICLE

Synthesis, preclinical evaluation, and a pilot clinical imaging study of [^{18}F]AlF-NOTA-JR11 for neuroendocrine neoplasms compared with [^{68}Ga]Ga-DOTA-TATE

Qing Xie[1] · Teli Liu[1] · Jing Ding[1] · Nina Zhou[1] · Xiangxi Meng[1] · Hua Zhu[1] · Nan Li[1] · Jiangyuan Yu[1] · Zhi Yang[1]

Received: 21 December 2020 / Accepted: 7 February 2021 / Published online: 25 February 2021

Abstract

Purpose A [^{18}F]AlF-labeled somatostatin receptor (SSTR) antagonist was developed for imaging of neuroendocrine neoplasms (NENs), evaluated and compared with [^{68}Ga]Ga-DOTA-TATE.

Method [^{18}F]AlF-NOTA-JR11 was synthesized manually and qualified with high-performance liquid chromatography (HPLC) and liquid chromatography–mass spectrometry (LC-MS). The cellular uptake, internalization, and saturation binding were performed with HEK293-SSTR2 cells. Biodistribution and micro-PET imaging were carried out with HEK293-SSTR2 tumor-bearing mice. [^{18}F]AlF-NOTA-JR11 PET/MR imaging and [^{68}Ga]Ga-DOTA-TATE PET/CT were performed with ten patients of NEN at 50~60 min post-injection (p.i.). Normal organ biodistribution and tumor detectability were evaluated.

Result [^{18}F]AlF-NOTA-JR11(24~36 GBq/μmol) was prepared within 30 min and 51.35 ± 3.30% ($n > 10$)of radiochemical yield. The radiochemical purity was 98.74 ± 1.24% ($n > 10$). Two stereoisomers were found and confirmed by LC-MS. The cellular uptake of [^{18}F]AlF-NOTA-JR11 and [^{68}Ga]Ga-DOTA-TATE were 4.50 ± 0.31 and 4.50 ± 0.13 %AD/10^5 cells at 30 min, and the internalization at 37 °C of [^{18}F]AlF-NOTA-JR11 (5.47 ± 0.32% at 60 min) was significantly lower than [^{68}Ga]Ga-DOTA-TATE (66.89 ± 1.62% at 60 min). The affinity of [^{18}F]AlF-NOTA-JR11 (K_d = 11.59 ± 1.31 nM) was slightly lower than [^{68}Ga]Ga-DOTA-TATE (K_d = 7.36 ± 1.02 nM); [^{18}F]AlF-NOTA-JR11 showed high uptake in tumor (9.02 ± 0.92 %ID/g at 60 min p.i.) which can be blocked by 50 μg of NOTA-JR11 (3.40 ± 1.64 %ID/g at 60 min p.i.); the result was coincident with micro-PET imaging. Imaging study of NEN patients showed that more lesions were found only by [^{18}F]AlF-NOTA-JR11 (n = 67 vs. 1 only by [^{68}Ga]Ga-DOTA-TATE), and the uptakes of [^{18}F]AlF-NOTA-JR11 in majority normal organs were significantly lower than [^{68}Ga]Ga-DOTA-TATE. The target to nontarget of maximum of standard uptake value (SUVmax) of [^{18}F]AlF-NOTA-JR11 in liver lesions were significantly higher than those of [^{68}Ga]Ga-DOTA-TATE.

Conclusion Qualitied [^{18}F]AlF-NOTA-JR11 is prepared conveniently with reasonable yield, and it can bind SSTR2 specifically with high affinity. Excellent imaging capability of [^{18}F]AlF-NOTA-JR11 for NENs is superior to [^{68}Ga]Ga-DOTA-TATE, especially in digestive system. It has a great potential for imaging of NENs.

Keywords Neuroendocrine neoplasms · Somatostatin receptor · AlF · Antagonist · PET imaging;

Introduction

Neuroendocrine neoplasms (NENs), which originate from endocrine cells of the spinal cord, are heterogeneous tumors that can secrete bioactive amines or multiple peptides [1]. Research by Modlin showed that 70~90% neuroendocrine tumors express somatostatin receptor (SSTR) [2], which is located on the cell membrane, and is a target of molecular imaging, somatostatin analogs (SSAs), and peptide receptor radionuclide therapy (PRRT) [3].

This article is part of the Topical Collection on Radiopharmacy

✉ Jiangyuan Yu
yujiangyuan@aliyun.com

✉ Zhi Yang
pekyz@163.com

[1] Department of Nuclear Medicine, Key Laboratory of Carcinogenesis and Translational Research, Ministry of Education, Peking University Cancer Hospital & Institute, No. 52 Fu-Cheng Rd., Beijing 100142, China

SSTR is a G protein coupled receptor that contains an intracellular region and extracellular region. When the somatostatin binds to the extracellular region of receptor, the receptor's intracellular region activates the downstream signaling followed by internalization of receptor ligand complex [4, 5]. At present, SSAs such as [^{99m}Tc]Tc-HYNIC-TOC [6], [^{68}Ga]Ga-DOTA-TATE [7], and [^{177}Lu]Lu-DOTA-TATE, which can activate signaling to lead to internalization and are known as SSTR agonists, have been successfully applied in nuclear medicine. In contrast, SSAs that cannot activate the signaling and lead to internalization, which are called antagonists, are in translational; these include [^{68}Ga]Ga-NODAGA-JR11, [^{68}Ga]Ga-DOTA-LM3, and [^{177}Lu]Lu-DOTA-JR11 [8–10]. A recent study [9] indicated that [^{68}Ga]Ga-OPS202 ([^{68}Ga]Ga-NODAGA-JR11) showed higher sensitivity in the detection of gastroenteropancreatic NENs than [^{68}Ga]Ga-DOTA-TOC.

SSTR agonist with [^{68}Ga]Ga (87% β^+, 0.83 MeV, $T_{1/2}$ = 68 min) is widely used in molecular imaging of NENs [11]. In addition, [^{68}Ga]Ga-DOTA-JR11 (SSTR antagonist) has already been applied in clinical imaging research [12]; however, the short half-life of [^{68}Ga]Ga and the low capacity of ^{68}Ge-^{68}Ga generator restrict the application of the radiolabeled products. In contrast, [^{18}F]F (97% β^+, 0.64 Mev, $T_{1/2}$ = 109 min) has a suitable half-life for peptide labeling and a shorter β^+-trajectory (<2 mm), leading to excellent imaging resolution [13]. Moreover, [^{18}F]F provided by a cyclotron can meet the needs of radiolabeling. The radiolabeling technology with "[^{18}F]AlF" has been applied successfully in research [14–17] and has enabled convenient labeling of peptides with [^{18}F]F$^-$. In 2020, human study of [^{18}F]AlF-NOTA-Octreotide was reported and firstly compared with [^{68}Ga]Ga-DOTA-TATE. The study indicated that [^{18}F]AlF-NOTA-Octreotide could be a qualified alternative for gallium-68-labeled SSA clinical PET imaging [18]. Though [^{18}F]SiFA-TATE was reported for somatostatin receptor imaging [19, 20], "AlF" technology seems superior to "SiFA" technology as its advantages of one-step reaction, and radiolabeling in aqueous solution rather than in organic solvent, which decreased the influence of residual solvent for safety.

This study reports the synthesis and quality analysis of [^{18}F]AlF-NOTA-JR11 (NOTA = 1,4,7-triazacyclononane-N,N′,N″-triacetic acid; JR11 = p-Cl-Phe-cyclo(D-Cys-Aph(Hor)-D-Aph(Cbm)-Lys-Thr-Cys)D-Tyr-NH_2) and evaluates its affinity and specificity in cells and tumor-bearing mice. Because PET/MR (positron emission tomography and magnetic resonance) has advantage in the diagnosis and staging of NENs in soft tissue [21], we designed a pilot clinical study to compare the biodistribution and lesion detectability between [^{18}F]AlF-NOTA-JR11 PET/MR imaging and [^{68}Ga]Ga-DOTA-TATE PET/CT imaging.

Materials and methods

Radiolabeling and quality analysis

The synthesis of [^{18}F]AlF-NOTA-JR11 is summarized in Fig. 1. Approximately 5~11.1 GBq [^{18}F]F$^-$(HM-20s Cyclotron, Sumitomo, Japan) was captured with a QMA SepPak light cartridge activated with 10 ml of 0.5 M $KHCO_3$ and 10 ml of metal-free water. [^{18}F]F$^-$ was eluted by 500 μl of 0.9% NaCl from a QMA column, and 100 μl of (1~2.2 GBq) [^{18}F]F$^-$ was added to reaction vial followed by 10 μl of KHP (0.5 M potassium hydrogen phthalate in metal-free water), 9 μl $AlCl_3$ (2 mM in 0.05 M KHP), and 10 μl of NOTA-JR11 (5 mg/ml in metal-free water). The vial was heated at 110 °C for 15 min. After cooling, the reaction liquid was applied to a C18 SepPak light cartridge activated by 10 ml of ethanol and 10 ml of water, and the cartridge was washed with 5 ml of water to remove the free [^{18}F]F$^-$ or [^{18}F]AlF^{2-}. Finally, [^{18}F]AlF-NOTA-JR11 was eluted and collected in 0.5 ml of 80% (v/v) ethanol and diluted with 0.9% NaCl. The radiochemical purity (RCP) was analyzed by radio-HPLC (high-performance liquid chromatography) on an Agilent 1200 system with a reversed-phase column (Agilent ZORBAX Eclipse Plus C18, 150 × 4.6 mm, 3.5 μm). A flow rate of 1 ml/min was used with mobile phase (consisting of 22% solution A and 78% solution B; solution A contained 0.1% (v/v) TFA (trifluoroacetic acid) in acetonitrile, and solution B contained 0.1% (v/v) TFA in water). The radioactivity was monitored by a B-Fc-1000 radiation detector (AR-2000, Bioscan, USA). Ultraviolet (UV) light detection was performed at a wavelength of 220 nm. [^{68}Ga]Ga-DOTA-TATE was obtained from the Department of Nuclear Medicine of Beijing Cancer Hospital.

The partition coefficient, pharmacokinetics, and stability in vitro and in vivo are shown in the supplemental materials.

The isolation and determination of stereoisomer

Because two radioactive peaks were observed for the [^{18}F]AlF-NOTA-JR11 purified by C18 cartridge with Radio-HPLC, semipreparative reverse-phase HPLC was used for separation. The chromatography condition was as follows: Alltima C18 (250 × 10 mm, 10 μm); 20% solution A, 80% solution B; flow rate, 5 ml/min. Two radioactive isolates were analyzed by radio-HPLC at 10, 20, 60, 120, and 180 min post-separation at room temperature.

To analyze and determine the two radioactive peaks, the stable nuclide [^{19}F]F$^-$ was used to synthesize [^{19}F]AlF-NOTA-JR11 by following a previous method, and liquid chromatography–mass spectrometry (LC-MS, micrOTOF-Q, BRUKER, Germany) was used to separate the two peaks and determine their molecular weight simultaneously. Due to the

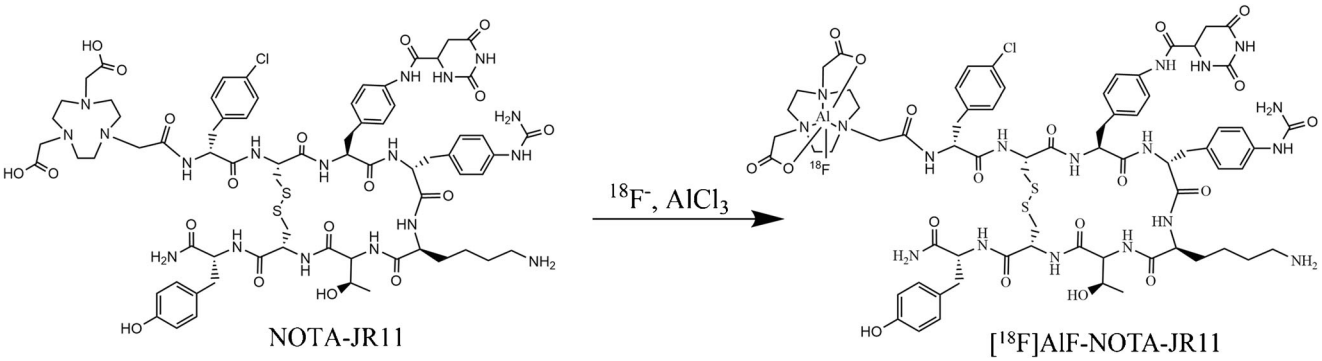

Fig. 1 The synthesis of [^{18}F]AlF-NOTA-JR11

decreased volatility of TFA in mass spectrometry, acetic acid was used in solution A and B instead of TFA. A reverse-phase column (Agilent ZOBAX Eclipse Plus C18, 100 × 4.6 mm,1.8 μm) was used in Waters 2795 system at a flow rate of 0.5 ml/min and a 220 nm UV wavelength, and the mobile phase contained 20% solution A and 80% solution B.

Cell uptake study

SSTR2(+) HEK293-SSTR2 cell line confirmed by western blot was obtained by HEK293 cell transfection. The detail of cell transfection was described in the supplemental materials. The transfected cells (1×10^5) were cultured in a 24-well plate overnight. Adherent cells were incubated with 500 μl of the culture medium, which was mixed with 300 μl of [^{18}F]AlF-NOTA-JR11(30 ± 5GBq/μmol) and 50 ml of serum-free DMEM (Dulbecco's Modified Eagle's Medium, Gibco Life Technologies, Gaithersburg, MD, USA), for 5, 30, 60, and 120 min. Inhibition for 60 and 120 min was performed in the presence of excess unlabeled NOTA-JR11 (25 μg). After incubation, the culture medium was removed and the cells were washed 2 times with cold PBS (0.01 M). Then, the cells were collected after digestion by 0.5 M NaOH and counted in a gamma counter. The percentage of added dose per 10^5 cells (%AD/10^5 cells) was calculated according to the count. The uptake study of [^{68}Ga]Ga-DOTA-TATE (27 ± 3 GBq/μmol) was performed using the same procedure.

Internalization of [^{18}F]AlF-NOTA-JR11 and [^{68}Ga]Ga-DOTA-TATE

Adherent cells (10^5) in 48-well plates were incubated with 300 μl of DMEM with 20 nM [^{18}F]AlF-NOTA-JR11 (30 ± 5 GBq/μmol) and [^{68}Ga]Ga-DOTA-TATE (27 ± 3 GBq/μmol) for 1 h at 4 °C and 37 °C. After incubation, the cells were washed once with cold PBS (0.01 M) and recultured with 300 μl of DMEM (time 0). At 0, 30, 60, and 120 min, the dissociation fraction from membrane was collected with culture medium, and the membrane-bound fraction (acid releasable) was separated by treating the cells with 0.1 M acetic acid in 0.01 M PBS (pH 2.85) for 5 min and then collected. The internalization fraction was collected after treating the cells with 0.5 M NaOH. All fractions (the dissociation fraction, the membrane-bound fraction, and the internalization fraction) were counted in γ-counter for calculating the rate of internalization [6, 22–24].

Saturation binding assay and K_d determination

Adherent cells (10^5) in 48-well plates were incubated in 300 μl of DMEM with increasing concentrations (0.05~150 nM) of [^{18}F]AlF-NOTA-JR11 (30 ± 5GBq/μmol) for 1 h at 4 °C. After incubation, the cells were washed 2 times with cold PBS (0.01 M) and collected after digestion with 0.5 M NaOH. The total binding was determined in a gamma counter. Nonspecific binding was determined in the presence of excess unlabeled NOTA-JR11 (10 μg). Specific binding was determined by subtracting nonspecific binding from the total binding. Prism Version 8.0 was used to calculate the K_d. The saturation binding of [^{68}Ga]Ga-DOTA-TATE (27 ± 3 GBq/μmol) was determined with the same procedure.

Immunohistochemistry

The liver, spleen, pancreas, and tumors dissected from HEK293-SSTR2 tumor-bearing mice were used for IHC assays with anti-somatostatin receptor 2 antibody (Abcam, UK). The IHC Imaging scanned with a Pannoramic DESK II DW (3D HISTECH, Hungary) and viewed by CaseViewer (3D HISTECH, Hungary). Additional details are provided in the supplemental materials.

Biodistribution

Twenty HEK293-SSTR2 tumor-bearing mice were randomly divided into five groups, with four in each group. The mice were injected with 1.85 MBq (30 ± 5 GBq/μmol) of [^{18}F]AlF-NOTA-JR11 intravenously and sacrificed at 5, 30, 60, and 120 min for organ collection. Fifty micrograms of NOTA-JR11 was coinjected with [^{18}F]AlF-NOTA-JR11 for

blocking. The organ weight and radioactivity counts were acquired to calculate the percentage of injected dose per gram (%ID/g) and the target to nontarget (T/NT) ratio. The biodistribution of [^{68}Ga]Ga-DOTA-TATE (27 ± 3 GBq/μmol) was performed following the same procedure.

Details of the establishment of HEK293-SSTR2 tumor bearing mice are provided in the supplemental material.

Micro PET/CT imaging of HEK293-SSTR2 tumor-bearing mice

After intravenous injection of [^{18}F]AlF-NOTA-JR11 (3.7 MBq, 30 ± 5 GBq/μmol) or [^{68}Ga]Ga-DOTA-TATE (3.7 MBq, 27 ± 3 GBq/μmol), imaging was performed with a micro PET/CT (Super Nova, PINGSHENG Healthcare, China) at 30 and 60 min. Inhibition imaging was performed after coinjection with 50 μg of NOTA-JR11 or DOTA-TATE. The maximum of standard uptake value (SUV_{max}) of the tumor was measured.

PET/CT and PET/MR imaging in patient with neuroendocrine neoplasms

The [^{18}F]AlF-NOTA-JR11 and [^{68}Ga]Ga-DOTA-TATE imaging studies were approved by the Ethics Committee of Beijing Cancer Hospital and Institute (permit 2020KT15 and 2014011313), and all individual participants signed an informed consent form. The safety evaluation of [^{18}F]AlF-NOTA-JR11 by the study of radiotoxicity in mice[Supplemental Fig. S4] was shown in supplemental materials and indicated that 150–200 MBq of [^{18}F]AlF-NOTA-JR11 was safe for human being. PET/CT (positron emission tomography and computed tomography) imaging of [^{68}Ga]Ga-DOTA-TATE and PET/MR imaging of [^{18}F]AlF-NOTA-JR11 were performed in the same patient on separate day within 3 ± 1.7 days. Ten patients (age 54.4 ± 8.77, range 38–68; Ki-67 18.6 ± 24.82, range 1–75) with pathologically confirmed NEN were included (Supplemental Table S1). Images were acquired 50~60 min post-injection of 150–200 MBq [^{68}Ga]Ga-DOTA-TATE (27 ± 3 GBq/μmol) and [^{18}F]AlF-NOTA-JR11 (30 ± 5 GBq/μmol), and PET images were analyzed by two experienced nuclear medicine physicians to measure the numbers and SUVmax of tumor lesions and the SUVmax of organs. Tumor lesions were confirmed by MRI of PET/MR. To avoid the influence of differences in equipment, the organs to muscles ratio of SUVmax was used to analyze the difference in distribution. For lesion evaluation, we used the target/nontarget (T/NT) ratio, which was the ratio of the highest SUVmax value of the primary tumor or metastases and the background. In addition, the radiation dosimetry of [^{18}F]AlF-NOTA-JR11 was estimated with the biodistribution date acquired from PET imaging in human which was performed with the imaging at different times, and the dosimetry (2.09 ± 0.71 mSv with 185 ± 13 MBq of injection) was acceptable. Additional details are given in the supplemental materials.

Statistics

SPSS Statistics (version 22.0 IBM) software was used to analyze the data. *P* value less than 0.05 indicated statistical significance.

Result

Radiolabeling, quality control, and stereoisomers

[^{18}F]AlF-NOTA-JR11 was labeled with a 51.35 ± 3.30% ($n > 10$) radiochemical yield. Radio-HPLC analysis (Fig. 2A) showed that the retention time of unbound "[^{18}F]AlF" was 1.77 min that was not observed (RCP <1%) during final production. The radiochemical purity was 98.74 ± 1.24% ($n > 10$). Two radioactivity peaks were found at 5.4 min (peak A) and 7.5 min (peak B), and the peak corresponding to NOTA-JR11 appeared at 7.41 min. After isolation with semipreparative reversed-phase HPLC, a single radioactivity peak was observed, which was followed by radio-HPLC analysis. The results (Fig. 2B) show that the two isolations were reciprocally transformed over time, and equilibrium (peak A: 65%; peak B: 35%) occurred after 120 min of isolation. LC-MS analysis of [^{19}F]AlF-NOTA-JR11 showed that the compounds corresponding to peak A and peak B separately had a similar mass spectrogram (Supplemental Fig. S1), and both had the same molecular weight (M = 1632). Therefore, [^{18}F]AlF-NOTA-JR11was used for further studies without separating isomers. The log $P_{octanol/water}$ value was calculated to determine the lipophilicity of [^{18}F]AlF-NOTA-JR11 and [^{68}Ga]Ga-DOTA-TATE. Log $P_{octanol/water}$ value of [^{18}F]AlF-NOTA-JR11 was −2.66 ± 0.031 ($n = 4$) and that of [^{68}Ga]Ga-DOTA-TATE was −3.06 ± 0.051 ($n = 4$), indicating that [^{18}F]AlF-NOTA-JR11 was less hydrophilic than [^{68}Ga]Ga-DOTA-TATE. The in vitro stability was determined in 0.9% NaCl and 5% HSA (human serum albumin). [^{18}F]AlF-NOTA-JR11 was stable in 0.9% NaCl and 5% HSA and was obtained at more than 95% of radiochemical purity within 6 h (Supplemental Fig. S2). The urine and blood of mice at 5 min p.i. and 30 min p.i. were obtained and analyzed by radio-HPLC for in vivo stability. The radiochemical purity of [^{18}F]AlF-NOTA-JR11 in urine was 97.15 ± 0.96% ($n = 4$, 5 min p.i.) and 96.76 ± 0.25% ($n = 4$, 30 min p.i.), and that in blood was 95.30 ± 3.5% ($n = 4$, 5 min p.i.). The radiochemical purity of [^{18}F]AlF-NOTA-JR11 in blood at 30 min p.i. was not detected because of rapid metabolism (Supplemental Fig. S3).

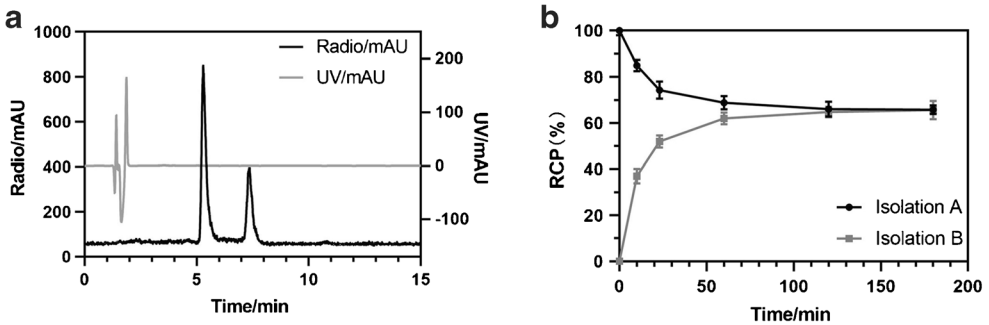

Fig. 2 A: radio-HPLC analysis of [^{18}F]AlF-NOTA-JR11; the mobile phase was a mixture of acetonitrile /0.1 %TFA (A) and water/0.1 %TFA (B), 22% A in 0–15 min, the flow rate was 1 ml/min. Radiochemical purity was more than 99% and no free [^{18}F]F ion was observed at 1.77 min. Two stereoisomers were observed and confirmed by LC-MS. B: the change of radiochemical purity of two isolation from semipreparative reversed-phase HPLC ($n = 3$). Isolation A was the collection of peak A (5.4 min); isolation B was the collection of peak B (7.5 min). RCP (radiochemical purity) of the first stereoisomer (5.4 min) was shown

Cellular uptake, internalization, and saturation binding assay

The cellular uptake (Fig. 3A) shows that the cellular uptake (4.50 ± 0.31 %AD/10^5 cells, $n = 4$) of [^{18}F]AlF-NOTA-JR11 reached a peak at 30 min and remained steady for 2 h, while the cellular uptake with unlabeled NOTA-JR11 was 0.18 ± 0.01 ($n = 4$) at 1 h and 0.16 ± 0.01 ($n = 4$) at 2 h and was significantly lower than the binding observed without unlabeled NOTA-JR11 ($p < 0.0005$). Compared with [^{18}F]AlF-NOTA-JR11, the cellular uptake of [^{68}Ga]Ga-DOTA-TATE was similar (4.50 ± 0.13, $n = 4$) at 30 min but increased steadily to 8.90 ± 0.50 ($n = 4$) within 2 h, while the cellular uptake with the unlabeled DOTA-TATE (0.32 ± 0.03, $n = 4$ at 1 h and 0.45 ± 0.03, $n = 4$ at 2 h) was significantly lower than the binding observed without unlabeled DOTA-TATE ($p < 0.0005$).

The internalization assay (Fig. 3B) (under the condition of incubation for 60 min) showed that the internalization rate of [^{18}F]AlF-NOTA-JR11 at 4 °C was 7.90 ± 1.10% ($n = 4$) at 0 min and was maintained at 120 min; however, the internalization rate of [^{68}Ga]Ga-DOTA-TATE was 22.42 ± 2.50% ($n = 4$) at 0 min and increased to 53.36 ± 4.07% ($n = 4$) at 120 min, significantly higher than that of [^{18}F]AlF-NOTA-JR11($p < 0.05$). The internalization rate of [^{68}Ga]Ga-DOTA-TATE at 37 °C was significantly higher than the rate at 4 °C ($p < 0.05$).

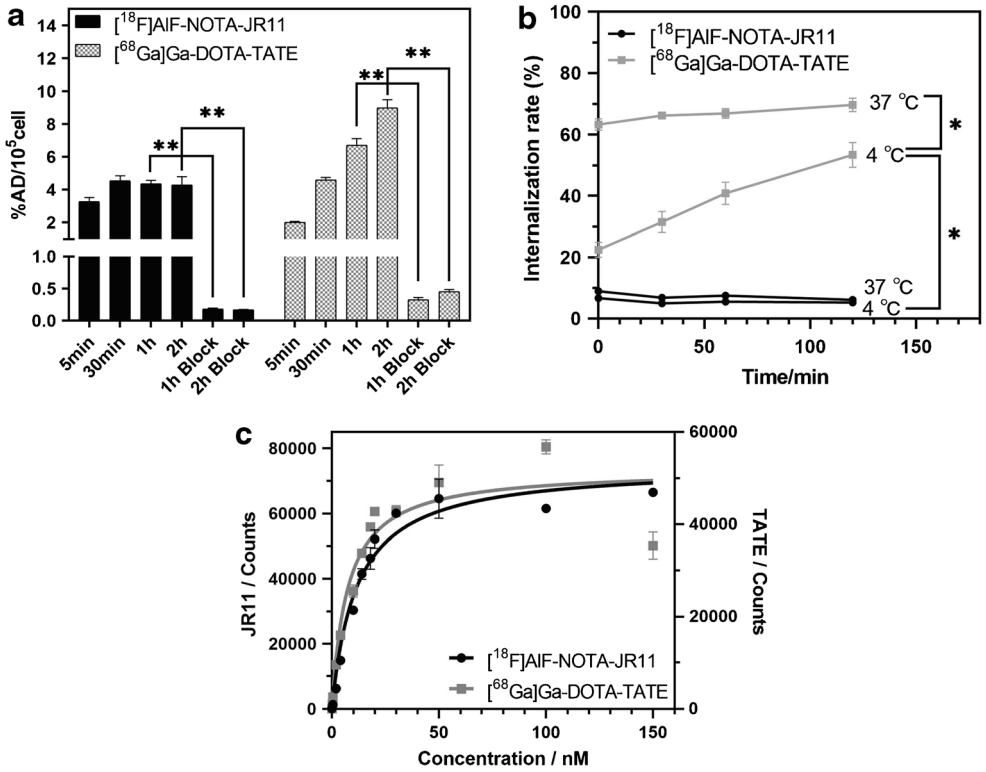

Fig. 3 A: the cellular uptake of [^{18}F]AlF-NOTA-JR11 and [^{68}Ga]Ga-DOTA-TATE, $n = 4$, $^{**}p < 0.0005$; %AD/10^5cells: the percentage of added dose per 10^5 cells. B: internalization of [^{18}F]AlF-NOTA-JR11 and [^{68}Ga]Ga-DOTA-TATE, $n = 4$; $^{*}p < 0.05$. C: saturation cell binding of [^{18}F]AlF-NOTA-JR11 ($K_d = 11.59 \pm 1.02$ nM) and [^{68}Ga]Ga-DOTA-TATE ($K_d = 7.36 \pm 1.31$ nM) at 4 °C, $n = 4$

The affinities of [^{18}F]AlF-NOTA-JR11 and [^{68}Ga]Ga-DOTA-TATE were determined with a saturation cell binding study at 4 °C (Fig. 3C). The K_d of [^{18}F]AlF-NOTA-JR11 ($K_d = 11.59 \pm 1.02$ nM, $n = 4$) was slightly higher than that of [^{68}Ga]Ga-DOTA-TATE ($K_d = 7.36 \pm 1.31$ nM, $n = 4$), indicating a lower affinity for SSTR2.

Immunohistochemistry

The expression of SSTR2 in tumor-bearing mice was determined by IHC (Supplemental Fig. S4B). The cell nuclei in the liver and spleen samples were stained blue by IHC, and the cell membranes were not stained brown, indicating that SSTR2 was not expressed in the liver and spleen. The cell membranes in the pancreas samples stained slightly brown, indicating low expressions of SSTR2. Obvious and intense brown staining was found in the cell membranes of HEK293-SSTR2 tumors, which confirmed overexpression of SSTR2.

Biodistribution

The biodistribution of [^{18}F]AlF-NOTA-JR11 and [^{68}Ga]Ga-DOTA-TATE was determined in HEK293-SSTR2 tumor-bearing mice and is illustrated with Table 1. The tumor uptake of [^{18}F]AlF-NOTA-JR11 was 9.02 ± 0.92 %ID/g at 60 min p.i., which was less than the tumor uptake of [^{68}Ga]Ga-DOTA-TATE (31.35 ± 5.9 %ID/g at 60 min p.i.). The tumor uptake of [^{18}F]AlF-NOTA-JR11 and [^{68}Ga]Ga-DOTA-TATE was decreased by coinjection of NOTA-JR11 and DOTA-TATE at 60 min p.i.(3.4 ± 1.64 %ID/g vs. 16.74 ± 3.4 %ID/g). Both [^{18}F]AlF-NOTA-JR11 and [^{68}Ga]Ga-DOTA-TATE were eliminated mainly by the kidney; however, compared with the high physiological uptake of [^{68}Ga]Ga-DOTA-TATE in the digestive system at 60 min p.i., including in the stomach (9.03 ± 4.99 %ID/g), small intestine (2.05 ± 1.22 %ID/g), large intestine (8.32 ± 1.59 %ID/g), and pancreas (20.69 ± 9.12 %ID/g), the physiological uptake of [^{18}F]AlF-NOTA-JR11 in the digestive system (1.09 ± 0.2, 1.27 ± 0.2, 1.02 ± 0.16, and 2.07 ± 0.42 %ID/g) was lower significantly ($p < 0.05$), and the T/NT ratios of these organs for [^{18}F]AlF-NOTA-JR11 were higher than those for [^{68}Ga]Ga-DOTA-TATE ($p < 0.05$). In addition, both [^{18}F]AlF-NOTA-JR11 and [^{68}Ga]Ga-DOTA-TATE exhibited slight uptake in bone (0.96 ± 0.03 %ID/g vs. 0.66 ± 0.17 %ID/g at 60 min p.i., $p > 0.05$).

Micro PET/CT imaging

Micro PET/CT imaging of [^{18}F]AlF-NOTA-JR11 and [^{68}Ga]Ga-DOTA-TATE in HEK293-SSTR2 tumor-bearing mice is shown in Fig. 4 A and B. There was high tumor uptake at 30 min p.i. and 60 min p.i., while the tumors observed in the inhibition imaging were almost invisible at 30 min p.i., indicating that accumulation of radioactivity was blocked by 50 μg of NOTA-JR11 or DOTA-TATE.

PET/CT and PET/MR imaging in patients with neuroendocrine neoplasms

During the imaging of [^{18}F]AlF-NOTA-JR11 and [^{68}Ga]Ga-DOTA-TATE, no treatment with SSA prior to the tracer injection was performed within 1 month. The biodistributions of [^{18}F]AlF-NOTA-JR11 and [^{68}Ga]Ga-DOTA-TATE in humans are shown in Fig. 5A. The uptake of [^{18}F]AlF-NOTA-JR11 in the liver, spleen, adrenal gland, intestine, and pancreas was significantly lower than that of [^{68}Ga]Ga-DOTA-TATE, but was higher in the blood and lungs ($p < 0.01$). The highest SUVmax values of lesions in the primary tumor and metastatic tumors were chosen to determine the T/NT ratio (Fig. 5B). The T/NT ratio according to the SUVmax of [^{18}F]AlF-NOTA-JR11 in the liver lesions was significantly higher than that of [^{68}Ga]Ga-DOTA-TATE ($p < 0.05$), and no significant difference was found among the other groups. The patient lesion information is shown in Fig. 5C. Because of the lower physiological uptake by the digestive system, [^{18}F]AlF-NOTA-JR11 scans detected more lesions of the primary and metastasis, especially liver metastases. Sixty-seven lesions were found only by [^{18}F]AlF-NOTA-JR11 scans, while just one lesion was found only by [^{68}Ga]Ga-DOTA-TATE scans. Only one bone lesion was missed in [^{18}F]AlF-NOTA-JR11 scans (patient 7, Fig. 6) compared with [^{68}Ga]Ga-DOTA-TATE. A typical case is shown in Fig. 7. More liver lesions were found by [^{18}F]AlF-NOTA-JR11. Furthermore, a primary tumor on the gastric wall was found by [^{18}F]AlF-NOTA-JR11 but not by [^{68}Ga]Ga-DOTA-TATE.

Discussion

SSTR has become an important target of clinical treatment and imaging in NET [3, 25]. Agonists of SSTR radiolabeled with [^{68}Ga]Ga and [^{99m}Tc]Tc, such as [^{68}Ga]Ga-DOTA-TATE and [^{99m}Tc]Tc-HYNIC-TOC, have been successfully applied in NEN imaging, while radiolabeled antagonists of SSTR, such as [^{68}Ga]Ga-DOTA-JR11 and [^{68}Ga]Ga-NODAGA-JR11, showed favorable diagnostic ability in clinical trials [9, 12, 26, 27]. The excellent physical characteristics of [^{18}F]F for imaging make it attractive for radiolabeling. A novel and rapid preparation method for radiolabeling with "[^{18}F]AlF" [13, 28, 29] was developed for peptides with high yield, meeting enough imaging needs. This study evaluated cellular uptake, the dissociation constant, internalization rate, biodistribution, and imaging of [^{18}F]AlF-NOTA-JR11

Table 1 The biodistribution of [^{18}F]AlF-NOTA-JR11 and [^{68}Ga]Ga-DOTA-TATE in HEK293-SSTR2 tumor-bearing mice

Organs	5 min (%ID/g)		30 min (%ID/g)		60 min (%ID/g)		120 min (%ID/g)		60 min-block (%ID/g)		60 min (T/NT)	
	JR11	TATE	JR11	TATE	JR11	TATE	JR11	TATE	JR11	TATE	JR11	TATE
Blood	9.06 ± 0.36	5.68 ± 0.84	1.33 ± 0.12	1.02 ± 0.15	0.58 ± 0.07	0.31 ± 0.03	0.26 ± 0.00	0.19 ± 0.03	1.08 ± 0.26	0.81 ± 0.01	16.01 ± 3.10	102.15 ± 21.23
Heart	2.96 ± 0.36	2.47 ± 0.25	0.8 ± 0.18	0.78 ± 0.19	0.42 ± 0.07	0.42 ± 0.04	0.17 ± 0.08	0.38 ± 0.04	0.64 ± 0.15	0.44 ± 0.05	22.01 ± 4.45	76.15 ± 21.21
Liver	2.79 ± 0.17	1.54 ± 0.13	1.17 ± 0.18	0.59 ± 0.11	0.73 ± 0.17	0.38 ± 0.02	0.57 ± 0.10	0.37 ± 0.03	0.68 ± 0.12	0.50 ± 0.02	12.82 ± 2.26	84.13 ± 19.67
Spleen	3.25 ± 0.61	2.55 ± 0.34	2.08 ± 0.48	1.55 ± 0.57	1.21 ± 0.32	0.86 ± 0.18	0.93 ± 0.08	0.7 ± 0.05	0.87 ± 0.14	0.60 ± 0.09	7.88 ± 1.61	36.56 ± 0.82
Lung	10.45 ± 0.93	12.74 ± 0.52	3.28 ± 0.73	6.10 ± 1.02	1.3 ± 0.36	3.25 ± 0.71	0.70 ± 0.06	4.39 ± 0.33	2.30 ± 0.38	1.02 ± 0.11	7.84 ± 3.24	10.23 ± 3.01
Kidney	26.10 ± 3.22	16.58 ± 1.37	11.5 ± 3.04	12.66 ± 4.90	11.45 ± 3.14	7.43 ± 0.92	11.38 ± 2.17	7.58 ± 1.31	24.64 ± 1.25	12.48 ± 0.81	0.86 ± 0.29	4.23 ± 0.66
Stomach	4.54 ± 0.15	14.08 ± 0.84	1.09 ± 0.20	9.28 ± 4.99	0.63 ± 0.28	9.03 ± 1.54	0.32 ± 0.12	9.61 ± 0.75	0.66 ± 0.50	0.56 ± 0.08	17.50 ± 7.70	3.52 ± 0.68
Small intestine	2.18 ± 0.17	3.97 ± 0.99	1.27 ± 0.20	2.76 ± 1.22	0.56 ± 0.05	2.05 ± 0.09	0.31 ± 0.22	2.01 ± 0.21	0.60 ± 0.16	0.49 ± 0.09	16.18 ± 1.27	15.23 ± 2.53
Large intestine	5.68 ± 0.66	12.99 ± 2.07	1.02 ± 0.16	9.62 ± 1.59	0.42 ± 0.08	8.32 ± 0.16	0.27 ± 0.07	6.73 ± 0.53	0.94 ± 0.16	0.56 ± 0.08	22.40 ± 5.63	3.76 ± 0.65
Muscle	2.04 ± 0.23	0.95 ± 0.45	0.52 ± 0.07	0.75 ± 0.49	0.25 ± 0.06	0.35 ± 0.07	0.18 ± 0.02	0.21 ± 0.02	0.56 ± 0.06	0.32 ± 0.04	37.16 ± 5.33	90.86 ± 7.70
Bone	2.65 ± 0.34	7.31 ± 2.18	1.09 ± 0.06	1.61 ± 0.66	0.96 ± 0.03	0.66 ± 0.17	1.00 ± 0.13	1.31 ± 0.06	1.64 ± 0.03	0.95 ± 0.15	9.44 ± 1.19	37.81 ± 2.95
Brain	0.21 ± 0.02	0.28 ± 0.03	0.07 ± 0.00	0.1 ± 0.02	0.04 ± 0.00	0.06 ± 0.01	0.04 ± 0.00	0.06 ± 0.00	0.08 ± 0.00	0.07 ± 0.00	206.36 ± 6.14	571 ± 184.97
Pancreas	7.83 ± 0.98	45.51 ± 4.87	2.07 ± 0.42	32.13 ± 9.12	0.84 ± 0.12	20.69 ± 1.53	0.27 ± 0.04	15.64 ± 1.02	0.55 ± 0.09	0.60 ± 0.04	11.07 ± 2.30	1.51 ± 0.22
Tumor	9.50 ± 0.90	12.7 ± 1.82	10.68 ± 2.05	29.72 ± 1.06	9.02 ± 0.92*	31.35 ± 5.90[§]	8.33 ± 0.83	27.3 ± 1.63	3.40 ± 1.64*	16.74 ± 3.40[§]		

%ID/g, percentage of injection dose per gram; *T/NT*, target to nontarget

Each group included four mice

*The tumor uptake blocked by NOTA-JR11 was significantly lower than the tumor uptake of [^{18}F]AlF-NOTA-JR11 at 60 min p.i. $p < 0.01$, $n = 4$

[§] The tumor uptake blocked by DOTA-TATE was significantly lower than the tumor uptake of [^{68}Ga]Ga-DOTA-TATE at 60 min p.i. $p < 0.05$, $n = 4$

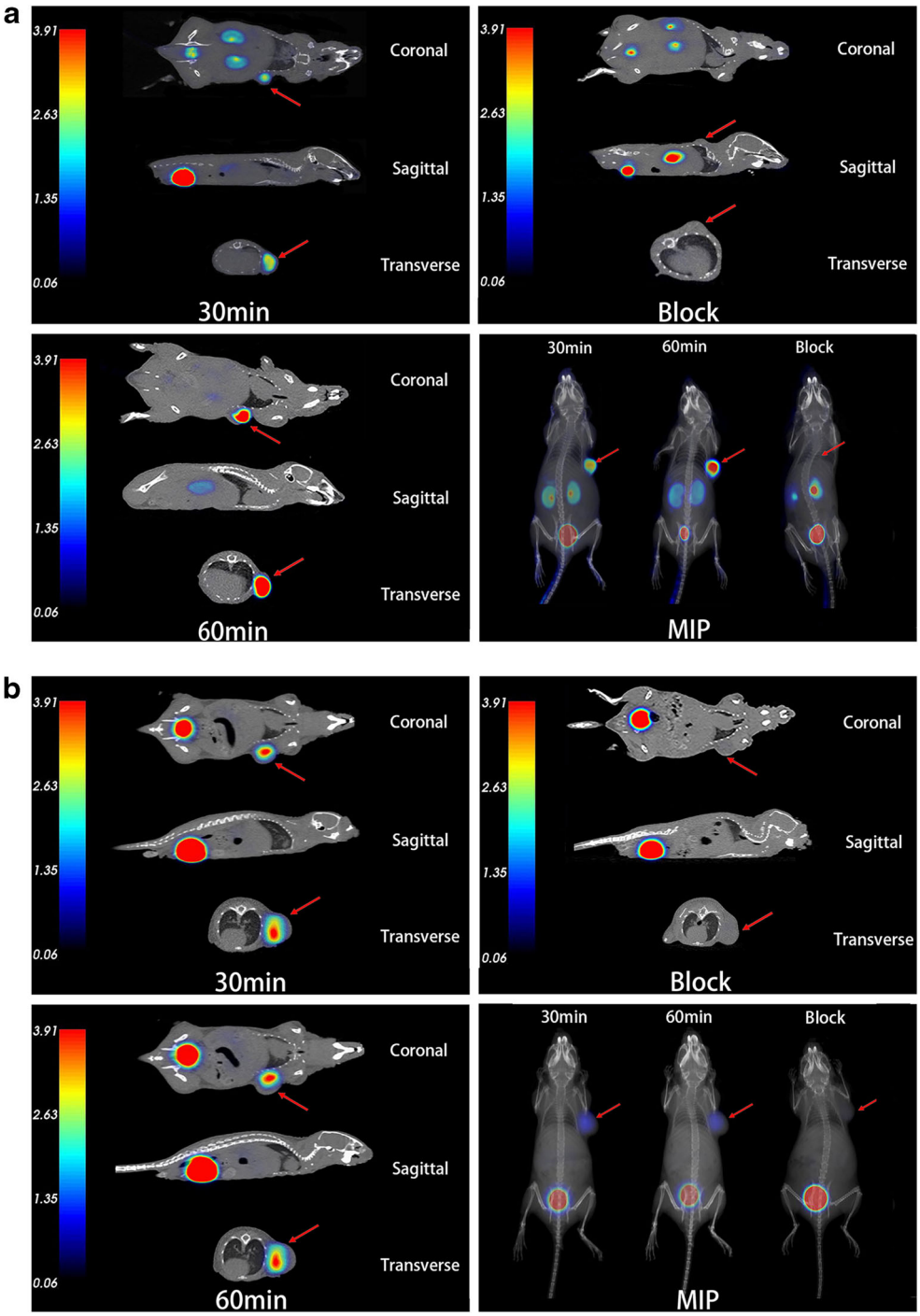

Fig. 4 A: the micro PET/CT imaging of [^{18}F]AlF-NOTA-JR11 in HEK293-SSTR2 tumor-bearing mice. Tumor: red arrow; SUVmax 2.49 at 30 min p.i., 3.77 at 60 min p.i., 0.35 (blocked by 50 μg NOTA-JR11) at 30 min p.i. B: the micro PET/CT imaging of [^{68}Ga]Ga-DOTA-TATE in HEK293-SSTR2 tumor-bearing mice. Tumor: red arrow; SUVmax 3.98 at 30 min p.i., 3.92 at 60 min p.i., 0.45 (blocked by 50 μg DOTA-TATE) at 30 min p.i. MIP, maximum intensity projection

compared with [^{68}Ga]Ga-DOTA-TATE, and this is a first report of a human study on [^{18}F]AlF-NOTA-JR11.

In this study, [^{18}F]AlF-NOTA-JR11 was prepared manually within 30 min, which was similar to preparation time of [^{68}Ga]Ga-DOTA-TATE. The radiochemical yield more than 50%, leading to the generation of 1.1 GBq of [^{18}F]AlF-NOTA-JR11 from 2.2 GBq of [^{18}F]F ion, was enough for imaging 5~6 patients. A massive dose of [^{18}F]AlF-NOTA-JR11 could be synthesized with an automatic synthesis procedure in future studies [30], which could allow clinical imaging of more patients. Quality control of [^{18}F]AlF-NOTA-JR11 was performed with radio-HPLC, and the tracer met the standard of the 2020 edition of the Chinese Pharmacopoeia for Clinical Application. The high stability of [^{18}F]AlF-NOTA-JR11 in 0.9% NaCl and 5% HSA allowed storage or short-distance transportation. Two radioactive peaks were observed and confirmed as stereoisomers by LC-MS; the

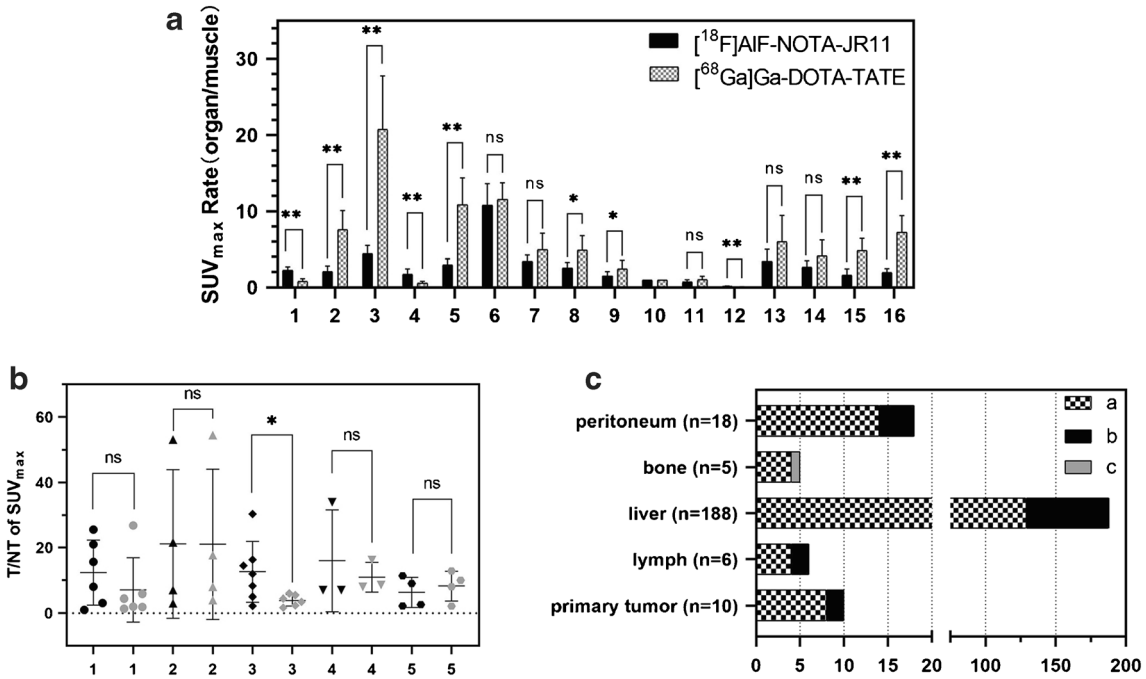

Fig. 5 A: the SUVmax rate of organ to muscle in NET patients, $n = 10$; ns: $p > 0.05$; *$p < 0.05$; **$p < 0.01$; 1: blood; 2: liver; 3: spleen; 4: lung; 5: adrenal gland; 6: kidney; 7: stomach; 8: duodenum; 9: colon; 10: muscle; 11: bone; 12: cerebellum; 13: hypophysis; 14: thyroid; 15: pancreatic body; 16: uncinate process of pancreas. B: target/nontarget (T/NT) of SUVmax of lesions in NET patients. The highest SUVmax of lesions with [^{68}Ga]Ga-DOTA-TATE and the same lesions with [^{18}F]AlF-NOTA-JR11 were chosen for the comparison. Black: [^{18}F]AlF-NOTA-JR11; Gray: [^{68}Ga]Ga-DOTA-TATE; 1: primary site; 2: lymph; 3: liver; 4: bone; 5:peritoneum. ns: $p > 0.05$; *$p < 0.05$. C: Numbers of lesions found by [^{18}F]AlF-NOTA-JR11 and [^{68}Ga]Ga-DOTA-TATE. a: lesions found by [^{18}F]AlF-NOTA-JR11 and [^{68}Ga]Ga-DOTA-TATE ($n = 159$); b: lesions found only by [^{18}F]AlF-NOTA-JR11 ($n = 67$); c: lesions found only by [^{68}Ga]Ga-DOTA-TATE ($n = 1$)

same phenomenon was associated with the synthesis of [^{18}F]AlF-IMP467 [29] and [^{18}F]AlF-NOTA-octreotide [31, 32]. Research by Christopher [13] demonstrated that the production of stereoisomers may be attributed to the hindered rotation of the complex with [^{18}F]F in an axial position in the NOTA-binding peptide.

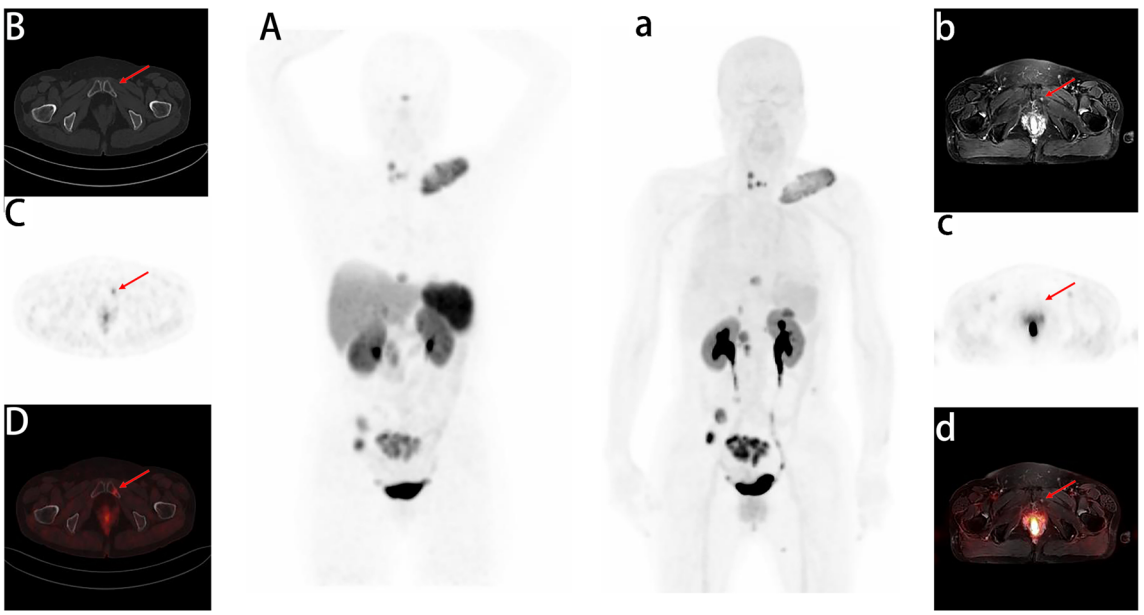

Fig. 6 A female (patient 7) with neuroendocrine lymph nodes and bone metastases G3. [^{68}Ga]Ga-DOTA-TATE imaging (A: MIP; B: CT; C: PET; D: PET/CT) showed a lesion of bone metastasis at the left of pubis (red arrow; SUVmax), while [^{18}F]AlF-NOTA-JR11 imaging (a: MIP; b: MRI; c: PET; d: PET/MR) missed the lesion. SUVmax of [^{68}Ga]Ga-DOTA-TATE: bone lesion 3.6; normal bone 1.1; SUVmax of [^{18}F]AlF-NOTA-JR11: bone lesion 0.6; normal bone 0.5

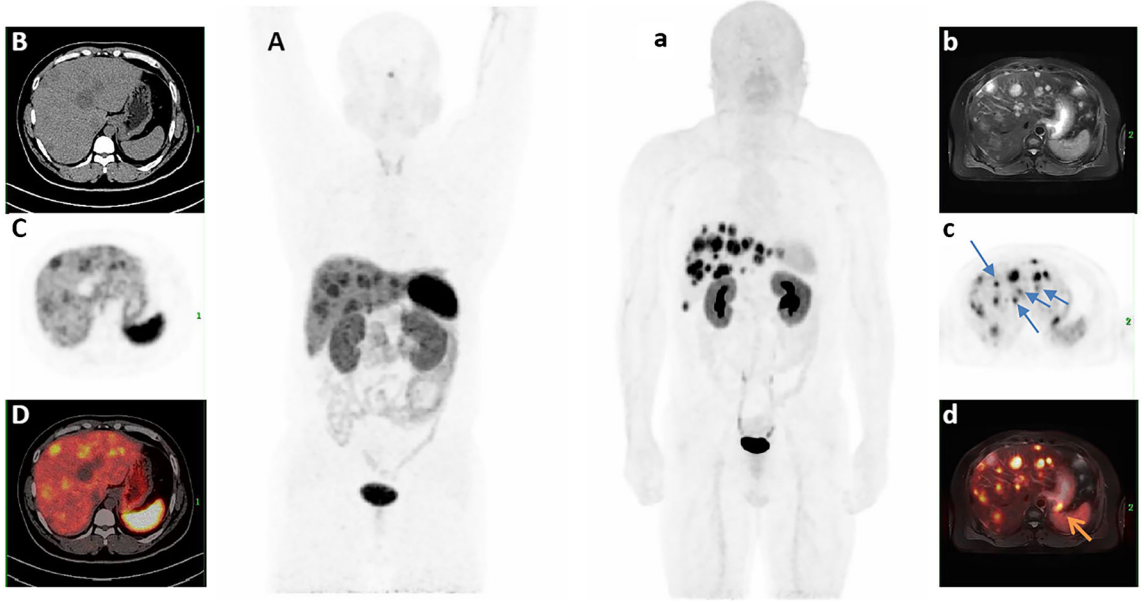

Fig. 7 A young male (patient 6) with neuroendocrine liver metastases G2. [^{68}Ga]Ga-DOTA-TATE imaging (A: MIP; B: CT; C: PET; D: PET/CT) showed multiple liver lesions with SSTR overexpression. While [^{18}F]AlF-NOTA-JR11 (a: MIP; b: MRI; c: PET; d: PET/MR) results found more hepatic foci (blue arrow) and located the primary in the gastric wall (yellow arrow). Following pathology from gastroscope certificated and Ki-67 was 5%. MIP, maximum intensity projection; T/NT of [^{18}F]AlF-NOTA-JR11: liver lesion 11.9; primary site 3.1. T/NT of [^{68}Ga]Ga-DOTA-TATE: liver lesion 2.3; primary site 1.3

Whether it led to internalization was one of the main differences between agonist and antagonist of SSTR. Compared to a previous study [24], the internalization rate of [^{68}Ga]Ga-DOTA-TATE (63.29 ± 1.87% at 37 °C after 60 min of incubation) in our study was higher, and that was 22.42 ± 2.5% at 4 °C. It may be attributed to extremely high overexpression of SSTR2 in HEK293-SSTR2 (211-fold higher than that of pancreas), which led to a higher probability of internalization. Another reason was that the enhanced adherence of HEK293-SSTR2 by poly-L-lysine decreased the loss of the cell by adding solutions. Uptake of [^{18}F]AlF-NOTA-JR11 by HEK293-SSTR2 cells was high and stable compared with the increasing uptake of [^{68}Ga]Ga-DOTA-TATE. Inhibition in the presence of unlabeled NOTA-JR11 (25 μg) confirmed the specificity of [^{18}F]AlF-NOTA-JR11 for SSTR2. The internalization assay demonstrated that the increase in the cellular uptake of [^{68}Ga]Ga-DOTA-TATE was due to the internalization of the complex of [^{68}Ga]Ga-DOTA-TATE and SSTR2, but it was not found in [^{18}F]AlF-NOTA-JR11. Therefore, to reduce the influence of internalization, a saturation cell binding assay was performed at 4 °C. The results showed that the affinity of [^{18}F]AlF-NOTA-JR11 for SSTR2 was high, but only slightly less than that of [^{68}Ga]Ga-DOTA-TATE. The dissociation constant (K_d) of [^{68}Ga]Ga-DOTA-TATE in this study was much higher (lower affinity) than that of [^{67}Ga]Ga-DOTA-TOC reported in past study [31]. However, it was in similar order to the affinity of JR11 and TATE according to IC_{50} (50% inhibitory concentration) [32, 33].

To evaluate expression of SSTR2 in HEK293-SSTR2 cells and tumors, western blot (Supplemental material) and IHC were performed. The results showed that both the cells and tumors were overexpressed SSTR2, and the expression of SSTR2 in murine pancreas and nonexpression of SSTR2 in the murine liver were consistent with the biodistribution of [^{68}Ga]Ga-DOTA-TATE (high uptake in the pancreas and low uptake in the liver). Moreover, tumor uptake of [^{18}F]AlF-NOTA-JR11 was lower than that of [^{68}Ga]Ga-DOTA-TATE, which was consistent with cellular uptake due to internalization and high affinity. Nonetheless, the lower uptake of [^{18}F]AlF-NOTA-JR11 by normal organs, especially in the digestive system, compared to that of [^{68}Ga]Ga-DOTA-TATE led to a clear imaging background that was convenient for diagnosis. Research by Fani [34] showed that uptake of [^{68}Ga]Ga-DOTA-JR11 (stomach 0.5 ± 0.1 %ID/g, pancreas 0.5 ± 0.1%ID/g at 60 min p.i.) in the digestive system was lower than that of [^{68}Ga]Ga-DOTA-TATE (stomach 8.6 ± 1.9 %ID/g, pancreas 10.8 ± 1.7 %ID/g at 60 min p.i.), which was similar to [^{18}F]AlF-NOTA-JR11, but that uptake of [^{68}Ga]Ga-NODAGA-JR11 (11.4 ± 3.6 %ID/g at 60 min p.i.) in the pancreas was similar to that of [^{68}Ga]Ga-DOTA-TATE (10.8 ± 1.7 %ID/g at 60 min p.i.). Compared with [^{68}Ga]Ga-NODAGA-JR11, [^{18}F]AlF-NOTA-JR11 had advantage in

detecting tumor in stomach and pancreas as its higher T/NT ratios in stomach (17.5 ± 7.70 vs. 3.1) and pancreas (11.07 ± 2.23 and 2.6). In addition, due to a lack of a significant difference in bone uptake of both tracers ($p > 0.05$) and a lack of bone uptake of [^{18}F]AlF-NOTA-JR11 in micro- PET imaging, it could be inferred that few or no free [^{18}F]F ions dissociated from [^{18}F]AlF-NOTA-JR11 in vivo. It was confirmed by the study of stability in vivo of [^{18}F]AlF-NOTA-JR11.

The excellent imaging contrast of [^{18}F]AlF-NOTA-JR11 led to the detection of more lesions with SSTR overexpression in the liver and digestive system. However, fewer lesions due to bone metastasis were detected by [^{18}F]AlF-NOTA-JR11, which suggests that [^{18}F]AlF-NOTA-JR11 is inferior for detecting metastatic lesions of the bone. Similar results were found for [^{68}Ga]Ga-DOTA-JR11 and [^{68}Ga]Ga-DOTA-TATE in 31 patients [12]. MR imaging has a superior soft tissue contrast compared to CT, which enables detailed evaluation of soft tissues within the abdomen, especially the liver. Moreover, MR imaging affords the opportunity to evaluate tissue function with diffusion-weighted imaging (DWI), MR spectroscopy, and perfusion-weighted imaging. Therefore, [^{18}F]AlF-NOTA-JR11 PET/MRI, as a new diagnostic modality, would show great potential value for the accurate staging of hepatic metastases, which is the most common metastatic type of NEN. Because this pilot study included only ten NEN patients to compare the biodistribution and lesion detection of [^{18}F]AlF-NOTA-JR11 and [^{68}Ga]Ga-DOTA-TATE, a larger number of samples should be assessed in the future followed by the dynamic imaging in mice and human, and the difference of SUVmax between [^{18}F]AlF-NOTA-JR11 and [^{68}Ga]Ga-DOTA-TATE would be analyzed in detail.

Conclusion

[^{18}F]AlF-NOTA-JR11 was obtained in 30 min with good yield and quality. A preclinical study of [^{18}F]AlF-NOTA-JR11 in cells and tumor-bearing mice demonstrated that [^{18}F]AlF-NOTA-JR11 can bind SSTR2 specifically with high affinity but with slightly lower affinity than [^{68}Ga]Ga-DOTA-TATE. The biodistribution and imaging in NEN patients indicated that [^{18}F]AlF-NOTA-JR11 is superior to [^{68}Ga]Ga-DOTA-TATE, especially in lesions of the digestive system, and has a great potential for NEN imaging.

Supplementary Information The online version contains supplementary material available at https://doi.org/10.1007/s00259-021-05249-8.

Funding This work was financially supported by National Natural Science Foundation of China projects (81871386, 81671733) and Natural Science Foundation of Beijing Municipality (7171002).

Declarations No other potential conflicts of interest relevant to this article exist.

All procedures performed in studies involving human participants were in accordance with the ethical standards of the institutional and/or national research committee and with the 1964 Helsinki declaration and its later amendments or comparable ethical standards. The study was approved by Ethics Committee of Beijing Cancer Hospital and Institute (permit 2,014,011,313 and 2020KT15). Informed consent was obtained from all individual participants included in the study.

References

1. Taal BG, Visser O. Epidemiology of neuroendocrine tumours. Neuroendocrinology. 2004;80(Suppl. 1):3–7.
2. Modlin IM, Pavel M, Kidd M, Gustafsson BI. Review article: somatostatin analogues in the treatment of gastroenteropancreatic neuroendocrine (carcinoid) tumours. Aliment Pharmacol Ther. 2010;31(2):169–88. https://doi.org/10.1111/j.1365-2036.2009.04174.x.
3. Pavel M, Baudin E, Couvelard A, et al. ENETS consensus guidelines for the management of patients with liver and other distant metastases from neuroendocrine neoplasms of foregut, midgut, hindgut, and unknown primary. Neuroendocrinology. 2012;95(2):157–76. https://doi.org/10.1159/000335597.
4. Waser B, Tamma ML, Cescato R, Maecke HR, Reubi JC. Highly efficient in vivo agonist-induced internalization of sst2 receptors in somatostatin target tissues [published correction appears in J Nucl Med. 2009 Oct;50(10):1578]. J Nucl Med. 2009;50(6):936–41. https://doi.org/10.2967/jnumed.108.061457.
5. Cescato R, Schulz S, Waser B, et al. Internalization of sst2, sst3, and sst5 receptors: effects of somatostatin agonists and antagonists. J Nucl Med. 2006;47(3):502–11.
6. Decristoforo C, Mather SJ, Cholewinski W, Donnemiller E, Riccabona G, Moncayo R. 99mTc-EDDA/HYNIC-TOC: a new 99mTc-labelled radiopharmaceutical for imaging somatostatin receptor-positive tumours; first clinical results and intra-patient comparison with 111In-labelled octreotide derivatives. Eur J Nucl Med. 2000;27(9):1318–25. https://doi.org/10.1007/s002590000289.
7. Gabriel M, Decristoforo C, Kendler D, Dobrozemsky G, Heute D, Uprimny C, et al. 68Ga-DOTA-Tyr3-octreotide PET in neuroendocrine tumors: comparison with somatostatin receptor scintigraphy and CT. J Nucl Med. 2007;48(4):508–18. https://doi.org/10.2967/jnumed.106.035667.
8. Wild D, Fani M, Fischer R, Del Pozzo L, Kaul F, Krebs S, et al. Comparison of somatostatin receptor agonist and antagonist for peptide receptor radionuclide therapy: a pilot study. J Nucl Med. 2014;55(8):1248–52. https://doi.org/10.2967/jnumed.114.138834.
9. Nicolas GP, Schreiter N, Kaul F, et al. Sensitivity comparison of 68Ga-OPS202 and 68Ga-DOTATOC PET/CT in patients with gastroenteropancreatic neuroendocrine tumors: a prospective phase II imaging study. J Nucl Med. 2018;59(6):915–21. https://doi.org/10.2967/jnumed.117.199760.
10. Fani M, Del Pozzo L, Abiraj K, et al. PET of somatostatin receptor-positive tumors using 64Cu- and 68Ga-somatostatin antagonists: the chelate makes the difference. J Nucl Med. 2011;52(7):1110–8. https://doi.org/10.2967/jnumed.111.087999.
11. Johnbeck CB, Knigge U, Loft A, et al. Head-to-head comparison of 64Cu-DOTATATE and 68Ga-DOTATOC PET/CT: a prospective study of 59 patients with neuroendocrine tumors. J Nucl Med. 2017;58(3):451–7. https://doi.org/10.2967/jnumed.116.180430.
12. Zhu W, Cheng Y, Wang X, et al. Head-to-head comparison of 68Ga-DOTA-JR11 and 68Ga-DOTATATE PET/CT in patients with metastatic, well-differentiated neuroendocrine tumors: a prospective study. J Nucl Med. 2020;61(6):897–903. https://doi.org/10.2967/jnumed.119.235093.

13. D'Souza CA, McBride WJ, Sharkey RM, Todaro LJ, Goldenberg DM. High-yielding aqueous 18F-labeling of peptides via Al18F chelation. Bioconjug Chem. 2011;22(9):1793–803. https://doi.org/10.1021/bc200175c.
14. McBride WJ, Sharkey RM, Goldenberg DM. Radiofluorination using aluminum-fluoride (Al18F). EJNMMI Res. 2013;3(1):36. Published 2013 May 8. https://doi.org/10.1186/2191-219X-3-36.
15. Chen Q, Meng X, McQuade P, et al. Synthesis and preclinical evaluation of folate-NOTA-Al(18)F for PET imaging of folate-receptor-positive tumors. Mol Pharm. 2016;13(5):1520–7. https://doi.org/10.1021/acs.molpharmaceut.5b00989.
16. Liu S, Liu H, Jiang H, Xu Y, Zhang H, Cheng Z. One-step radiosynthesis of ^{18}F-AlF-NOTA-RGD$_2$ for tumor angiogenesis PET imaging. Eur J Nucl Med Mol Imaging. 2011;38(9):1732–41. https://doi.org/10.1007/s00259-011-1847-4.
17. McBride WJ, Sharkey RM, Karacay H, et al. A novel method of 18F radiolabeling for PET. J Nucl Med. 2009;50(6):991–8. https://doi.org/10.2967/jnumed.108.060418.
18. Pauwels E, Cleeren F, Tshibangu T, Koole M, Serdons K, Dekervel J, et al. [18F]AlF-NOTA-octreotide PET imaging: biodistribution, dosimetry and first comparison with [68Ga]Ga-DOTATATE in neuroendocrine tumour patients. Eur J Nucl Med Mol Imaging. 2020 Dec;47(13):3033–46. https://doi.org/10.1007/s00259-020-04918-4.
19. Niedermoser S, Chin J, Wängler C, Kostikov A, Bernard-Gauthier V, Vogler N, et al. In vivo evaluation of ^{18}F-SiFAlin-modified TATE: a potential challenge for ^{68}Ga-DOTATATE, the clinical gold standard for somatostatin receptor imaging with PET. J Nucl Med. 2015;56(7):1100–5. https://doi.org/10.2967/jnumed.114.149583.
20. Ilhan H, Lindner S, Todica A, Cyran CC, Tiling R, Auernhammer CJ, et al. Biodistribution and first clinical results of 18F-SiFAlin-TATE PET: a novel 18F-labeled somatostatin analog for imaging of neuroendocrine tumors. Eur J Nucl Med Mol Imaging. 2020;47(4):870–80. https://doi.org/10.1007/s00259-019-04501-6.
21. Paspulati RM, Gupta A. PET/MR imaging in cancers of the gastrointestinal tract. PET Clin. 2016;11(4):403–23. https://doi.org/10.1016/j.cpet.2016.05.004.
22. Sato N, Hassan R, Axworthy DB, Wong KJ, Yu S, Theodore LJ, et al. Pretargeted radioimmunotherapy of mesothelin-expressing cancer using a tetravalent single-chain Fv-streptavidin fusion protein. J Nucl Med. 2005;46(7):1201–9.
23. Misri R, Saatchi K, Ng SS, Kumar U, Häfeli UO. Evaluation of (111)in labeled antibodies for SPECT imaging of mesothelin expressing tumors. Nucl Med Biol. 2011;38(6):885–96. https://doi.org/10.1016/j.nucmedbio.2011.02.013.
24. Schottelius M, Šimeček J, Hoffmann F, Willibald M, Schwaiger M, Wester HJ. Twins in spirit - episode I: comparative preclinical evaluation of [(68)Ga]DOTATATE and [(68)Ga]HA-DOTATATE. EJNMMI Res. 2015;5:22. https://doi.org/10.1186/s13550-015-0099-x.
25. Bozkurt MF, Virgolini I, Balogova S, et al. Guideline for PET/CT imaging of neuroendocrine neoplasms with 68Ga-DOTA-conjugated somatostatin receptor targeting peptides and 18F-DOPA. Eur J Nucl Med Mol Imaging. 2017;44(9):1588–601. https://doi.org/10.1007/s00259-017-3728-y.
26. Nicolas GP, Beykan S, Bouterfa H, et al. Safety, biodistribution, and radiation dosimetry of 68Ga-OPS202 in patients with gastroenteropancreatic neuroendocrine tumors: a prospective phase I imaging study. J Nucl Med. 2018;59(6):909–14. https://doi.org/10.2967/jnumed.117.199737.
27. Krebs S, Pandit-Taskar N, Reidy D, et al. Biodistribution and radiation dose estimates for 68Ga-DOTA-JR11 in patients with metastatic neuroendocrine tumors. Eur J Nucl Med Mol Imaging. 2019;46(3):677–85. https://doi.org/10.1007/s00259-018-4193-y.
28. Liu T, Liu C, Xu X, Liu F, Guo X, Li N, Wang X, Yang J, Yang X, Zhu H, Yang Z. Preclinical evaluation and pilot clinical study of Al^{18}F-PSMA-BCH for prostate cancer PET imaging. J Nucl Med. 2019;60(9):1284-1292. doi: https://doi.org/10.2967/jnumed.118.221671. [29] McBride WJ, D'Souza CA, Sharkey RM, et al. Improved ^{18}F labeling of peptides with a fluoride-aluminum-chelate complex. Bioconjug Chem 2010;21(7):1331–1340. doi: https://doi.org/10.1021/bc100137x.
29. McBride WJ, D'Souza CA, Sharkey RM, et al. Improved ^{18}F labeling of peptides with a fluoride-aluminum-chelate complex. Bioconjug Chem. 2010;21(7):1331–40. https://doi.org/10.1021/bc100137x.
30. Tshibangu T, Cawthorne C, Serdons K, Pauwels E, Gsell W, Bormans G, et al. Automated GMP compliant production of [18F]AlF-NOTA-octreotide. EJNMMI Radiopharm Chem. 2020;5(1):4. https://doi.org/10.1186/s41181-019-0084-1.
31. Laverman P, McBride WJ, Sharkey RM, et al. A novel facile method of labeling octreotide with (18)F-fluorine. J Nucl Med. 2010;51(3):454–61. https://doi.org/10.2967/jnumed.109.066902.
32. Reubi JC, Schär JC, Waser B, et al. Affinity profiles for human somatostatin receptor subtypes SST1-SST5 of somatostatin radiotracers selected for scintigraphic and radiotherapeutic use. Eur J Nucl Med. 2000;27(3):273–82. https://doi.org/10.1007/s002590050034.
33. Cescato R, Erchegyi J, Waser B, et al. Design and in vitro characterization of highly sst2-selective somatostatin antagonists suitable for radiotargeting. J Med Chem. 2008;51(13):4030–7. https://doi.org/10.1021/jm701618q.
34. Fani M, Braun F, Waser B, et al. Unexpected sensitivity of sst2 antagonists to N-terminal radiometal modifications. J Nucl Med. 2012;53(9):1481–9. https://doi.org/10.2967/jnumed.112.102764.